New Internal-Charge-Transfer Second Order NLO Chromophores based on the donor Ferrocenylpyrazole Moiety

Kabali Senthilkumar,[†] Maddalena Pizzotti,[‡*] Krishnan Thirumoorthy,[†] Gabriele Di Carlo,[‡] Stefania Righetto,[‡] Alessio Orbelli Biroli,[§] Matti Haukka,[‖] Nallasamy Palanisami[†*]

† Department of Chemistry, School of Advanced Sciences, VIT University, Vellore 632014, Tamil Nadu, India.

‡ Department of Chemistry, University of Milan, INSTM Research Unit, Via C. Golgi 19, 20133 Milan, Italy.

§ Istituto di Scienze e Tecnologie Molecolari del CNR (CNR-ISTM) Via C. Golgi 19, 20133 Milan, Italy

‖ Department of Chemistry, University of Jyväskylä, P.O. Box 35, FI-40014 Jyväskylä, Finland.

Corresponding Authors

*Nallasamy Palanisami: Email: palanisami.n@gmail.com; Tel: +91 9842639776

*Maddalena Pizzotti: Email: maddalena.pizzotti@unimi.it; Tel: 02503 14363

Abstract

A series of new N-arylated ferrocenepyrazole structures, carrying different donor or acceptor substituents in the para position of the aryl ring has been synthesized by the Chan-Lam cross coupling reaction. The nonplanar geometric molecular structure of some of these chromophores together with their crystal packing was determined by X-ray diffraction and the HOMO and LUMO energy levels were evaluated by electrochemical and optical measurements and by DFT theoretical calculations. By the investigation of solvent effects and TD-DFT calculations the intense electronic absorption band at around 270-310 nm was confirmed to be an internal-charge-transfer (ICT) band, showing a significant red shift by increasing the electron withdrawing properties of the substituent on the para position of the aryl ring. TD-DFT calculations and EFISH measurements of the quadratic hyperpolarizability have shown that also the second order NLO response of these new ICT chromophores can be tuned by changing the nature of the substituent. Both theoretical $\mu\beta$, β and experimental EFISH $\mu\beta_{1907}$ and β_{1907} values are significant, with a quite satisfactory correlation of the general trend of theoretical $\mu\beta$ and EFISH $\mu\beta_{1907}$ values. The highest value of EFISH $\mu\beta_{1907}$ (410 x 10^{-48} esu) was measured for the chromophore carrying the strong electron withdrawing NO_2 group.

Introduction

Due to the potential applications in optical communications, data storage, field effect transistors, light emitting diodes, and dye-sensitized solar cells, molecular structures including electron-acceptor (A) and electron-donor (D) groups were extensively investigated as new functional materials.[1] Asymmetric organic or organometallic push-pull structures or molecular species characterised by internal-charge-transfer (ICT) processes, which have dipolar electronic structures, are potentially interesting nonlinear optical (NLO) molecular materials.[2] In particular examples of intramolecular charge-transfer excitations, affording large dipole moment changes $\Delta\mu_{eg}$ (difference between excited-state and ground-state dipole moments), as origin of significant quadratic hyperpolarizability (β) and of quadratic electro-optic effect (QEO effect) have been reported.[3] Modulation of the charge-transfer processes in organometallic chromophores has provided excellent opportunities for tuning the second order nonlinear optical response,[4] so that push-pull and ICT organometallic chromophores based for instance on metals such as iron and ruthenium have been largely investigated.[5] Ferrocene has an ionization energy and redox electrochemical potentials comparable to those of the best organic donors,[6] together with a high chemical stability of both the neutral (Fe^{2+}) and cationic (Fe^{3+}) species with a facile interconversion between the two oxidation states.[7] Therefore, it has been investigated as an ideal organometallic donor building block for mixed-valence organometallic species,[8] magnetic charge-transfer,[9] photo-induced charge transfer,[10] and redox-active sensors for cations and anions detections.[11] Hence ferrocene, the first organometallic species reported as donor moiety for second-order NLO chromophores,[4g] remains one of the most widely investigated donor species, comparable to N,N′-dimethyl, and methoxyphenyl organic donors. A significant series of investigations have been devoted to push-pull chromophores where the donor properties of ferrocene are due to the electronic coupling between the metal d-orbitals and the π-network of the donor-acceptor linker of the push-

pull structure.[6, 12] Second order NLO chromophores involving the ferrocenyl moiety as the donor part of an ICT process have been much less investigated.

Pyrazoles are five-membered heterocyclic structures investigated as promising donor moieties for organic second-order NLO chromophores. Moreover, they may find applications in optical laser technology,[13] or as an electroluminescent source.[14] Blue emitting fluorescent dyes based on pyrazole structure characterized by high fluorescence quantum yield have been also reported.[15] Second order NLO properties of several pyrazole derivatives were investigated, showing relatively good β values.[16,17] For instance Miller et al.[18] have reported the first organic ICT chromophores based on an N-arylated pyrazolic structure, characterized by a quite good second order NLO response measured by EFISH technique. Moreover Zilio et al.[19] measured, by the HRS techniques, a β value of 45 ± $2x10^{-30}$ esu for a second order NLO organic chromophore based on a substituted pyrazole. New pyrazole based push-pull second order NLO chromophores are reported to exhibit excellent values of both ground state dipole moments and quadratic hyperpolarizability.[20]

The present work focuses on the synthesis and on the structural, spectroscopic, electrochemical, theoretical and second order NLO characterization of ICT chromophores based on N-arylated ferrocenyl pyrazole derivatives [1-(4-R-phenyl)-5-methyl-3-ferrocenyl-1H-pyrazole (R = H, *tert*-butyl, Ph, $CO(CH_3)$, CHO, Cl, F, CF_3, CN, NO_2, OMe, NMe_2)]. These chromophores have been synthesized by the Chan-Lam coupling reaction[21] in good yields and characterized by microanalysis, FT-IR, FT-NMR and mass spectrometry. Their structures have been confirmed by single crystal X-ray diffraction (XRD) and their electronic absorption spectra and electrochemical properties have been experimentally investigated and theoretically analyzed by DFT and TD-DFT methods. Their second order NLO responses were experimentally measured by means of the EFISH technique and theoretically calculated by the TD-DFT approach.

Results and Discussion

Synthesis, physicochemical and crystallographic characterization

The starting material [3-ferrocenyl-5-methyl-1H-pyrazole] was prepared by reaction of a ferrocenyl *β*-diketone ($FcCOCHCOCH_3$)[22] with hydrazine hydrate (1:1 ratio) according to the literature.[23] Many synthetic routes for the synthesis of N-arylated pyrazole derivatives involve the condensation of N-arylated hydrazine with the *β*-diketone moiety, while alternative routes involving a C-N coupling reaction were developed by using NaH,[24] Cs_2CO_3 and K_2CO_3 based Cu catalysts[25] and Zn-Li[26] based catalysts. However, our attempts to synthesize by these routes N-arylated ferrocenyl pyrazoles were unsuccessful. Therefore, we synthesized these molecules following the Chan-Lam coupling reaction[21] which is a copper salt-promoted cross coupling (scheme 1). The reaction proceeds under relatively mild conditions independently from the nature of the substituents on the phenyl ring. A possible reaction mechanism is reported in scheme 1 while details are given in the Supporting Information. The Chan-Lam coupling reaction proceeds stereo and regioselectively with excellent yields by copper catalyzed N-arylation of ferrocenyl-5-methyl-1H-pyrazole. The products [1-(4-R-phenyl)-5-methyl-3-ferrocenyl-1H-pyrazole (R = H, *tert*-butyl, Ph, $COCH_3$, CHO, Cl, F, CF_3, CN, NO_2, OMe, NMe_2] were obtained by reaction of [3-ferrocenyl-5-methyl-1H-pyrazole] in CH_2Cl_2 solution with various arylboronic acids in the presence of copper^{II} acetate, pyridine and 4Å molecular sieves (see supporting Information). All the chromophores were unambiguously characterized by FT-IR, FT-NMR and Electron Ionization (EI)-mass spectroscopies. The pyrazole moiety could allow the formation of regioisomers, but for all the chromophores investigated (**1**-**12**) (see Scheme 1) one major regioisomer was predominant. The minor regioisomer produced in low yield (<5%), was easily separated by column chromatography. The thermogravimetric analysis confirmed a thermal stability in the air up to 300 ˚C (see TGA of **8** and **9** reported in Figure S1), so that all the chromophores could be stored without special precautions. The structures of

chromophores **5**, **7**, **8** and **9** were fully characterized by single crystal X-ray diffraction (Table S1 and Figure 1) and by ^{1}H NMR spectroscopy

.

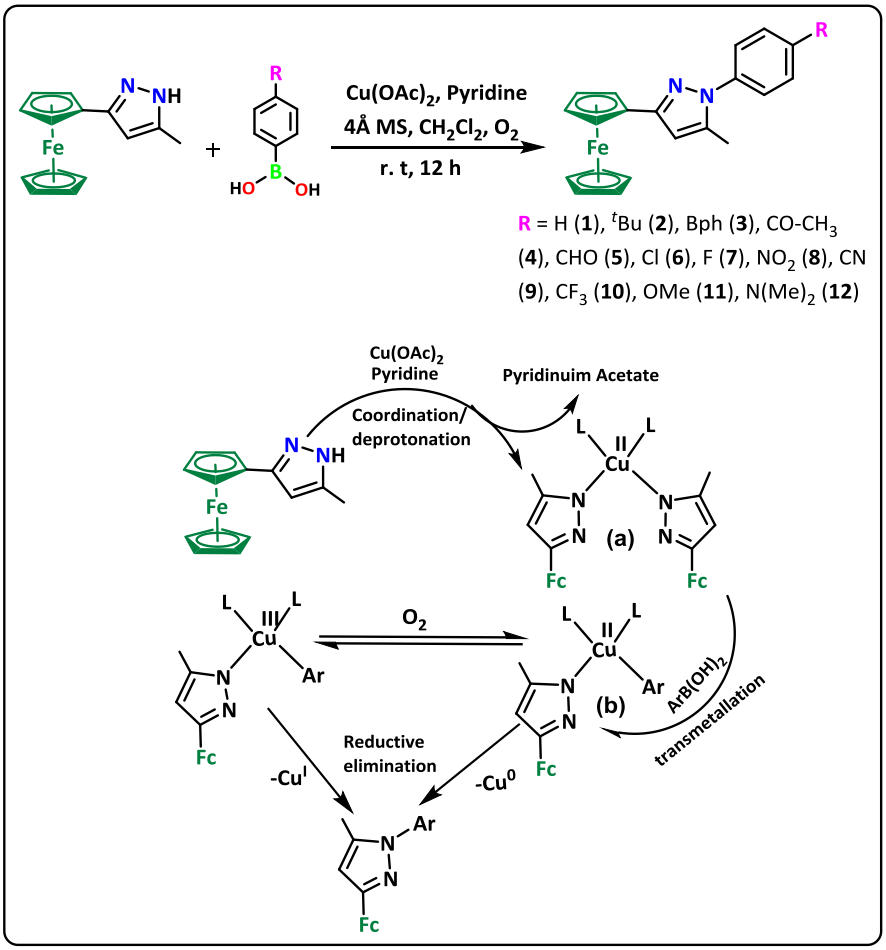

Scheme 1. The Chan-Lam synthesis of chromophores **1-12** and a possible reaction mechanism.

The C-N coupling bond formation for chromophores **5, 7, 8** and **9** at the desired nitrogen atom was confirmed by crystals grown by recrystallization from different mixed solvents (CH_3OH, $CHCl_3$, and CH_2Cl_2) at room temperature. The structures of **5**, **7**, **8** and **9** are shown in Figure 1 with the appropriate atom numbering. The data collections, structure refinement as well as the parametric data of the unit cells are given in Table S1, whereas Table 1 contains the most relevant bond lengths, bond angles and dihedral angles for **5**, **7**, **8** and **9**. All the chromophores crystallize in the

centrosymmetric space groups (**5**, **7** and **9**: monoclinic P lattice with $P2_1/c$; **8**: monoclinic P lattice with $P2_1/n$), thus, they are not expected to show any bulk nonlinear optical property.[4b, 4h, 27]

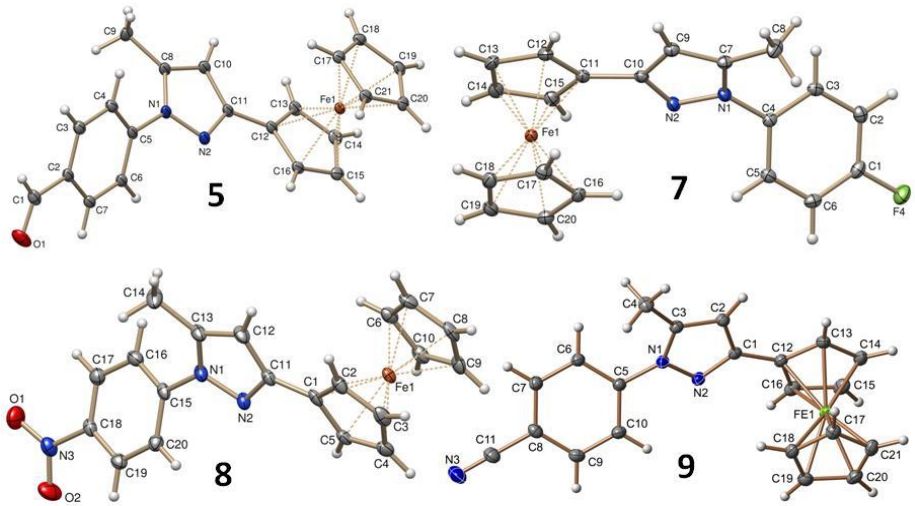

Figure 1. Representation of the crystallographic molecular structure of chromophores **5**, **7**, **8** and **9** (with 30% probability ellipsoids), with numbering of C, N, O, F and Fe atoms.

The crystal packing of chromophores **5, 7-9** shows the antiparallel alignment of the neighboring chromophores; the overlap pictograms of the aromatic rings and other inter and intra-atomic interactions are shown in Figures S2-S7 and exhibit inter and intramolecular interactions *via* hydrogen bonding and π-π interactions. For instance **5** shows a hydrogen bonding network *via* C-H···O contacts particularly stabilized by π····π (3.362 Å) and C-H····π (3.385 Å) interactions involving the cyclopentadienyl ring as shown in (Figure S3), while **7** shows strong H-F bonding of 2.455 and 2.961 Å between two adjacent rings, with a stabilisation of a sheet-like structure (Figure 2).

The geometric parameters of all the chromophores are closely related[28] and characterized by a slight twist angle between the cyclopentadienyl ring of ferrocenyl and the pyrazole ring, and with a torsion angle between the pyrazole and the aromatic rings. It follows that the arrangement of the

total π structure is not planar, although the arrangement between the cyclopentadienyl ring of the ferrocenyl and the pyrazole moieties is slightly planar (Figure 3). As shown in Figure 3 the lack of planarity of the structures of **5, 7-9** is measured by their cyclopentadienyl-pyrazole twist angle and by their torsion or dihedral angles ϕ_1 and ϕ_2 between the ferrocenylpyrazole moieties and the substituted phenyl ring respectively.

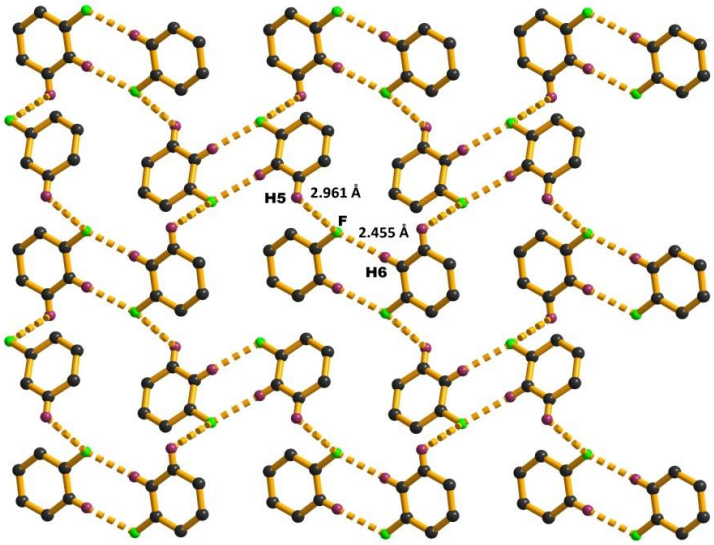

Figure 2. Core sheet-like formation by H····F bonding in the crystal structure of **7**, with H····F hydrogen bond distances of 2.455 and 2.961 Å.

A pictorial representation of the values (given in Table 1) of ϕ_1 and ϕ_2 is reported in Figure S8. The torsion between the plane of the pyrazole and the phenyl ring reduces the π interaction and therefore the intramolecular charge-transfer process which should control the molecular second-order NLO response.[29] As reported in Table 1 the values of angles ϕ_1 and ϕ_2 indicate that the aromatic and pyrazole rings are quite twisted in all the chromophores as confirmed by DFT optimized structures of **1, 7-12** reported in Figure S10.

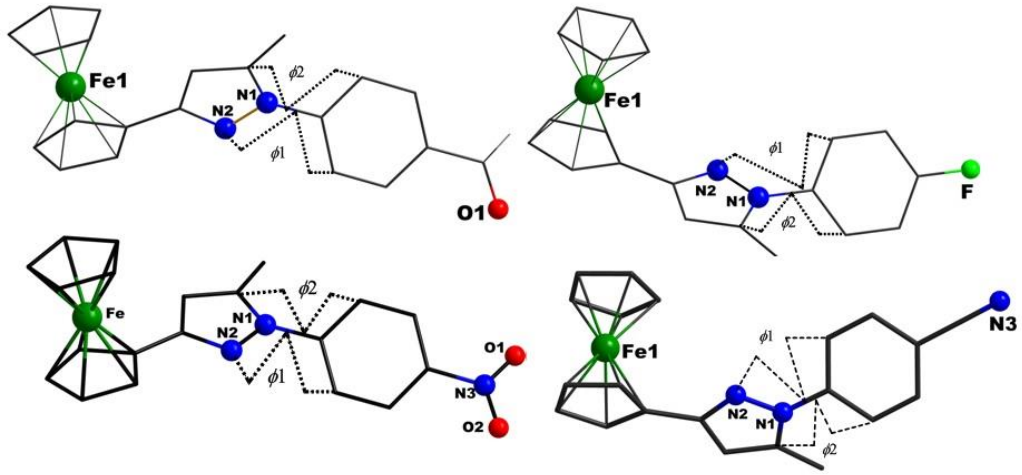

Figure 3. Dihedral or torsion angle ϕ_1 and ϕ_2 of **5, 7, 8** and **9**.

Table 1. Relevant structural parameters of **5**, **7**, **8** and **9**. The interatomic distances are reported in Å, angles in degrees.

Chromophore	**5**	**7**	**8**	**9**
Average Fe-C	2.052(4)	2.046(9)	2.049(9)	2.046(2)
Fe-Cent(1)	1.655(5)	1.648(0)	1.650(2)	1.648(3)
Fe-Cent(2)	1.651(5)	1.646(2)	1.653(4)	1.646(0)
Cent(1)-Fe(1)-Cent(2)	177.72(3)	178.95(9)	178.35(8)	179.22(8)
N(1)-N(2)	1.370(9)	1.370(3)	1.372(7)	1.371(3)
N(1)-C(8)	1.372(1)	1.368(2)	1.373(8)	1.370(2)
N(1)-C(5)	1.416(1)	1.422(5)	1.413(3)	1.408(8)
N(2)-C(11)	1.335(1)	1.338(6)	1.331(6)	1.333(8)
C(11)-C(12)-N(1)	157.89(3)	160.16(0)	158.27(5)	160.22(5)
C(11)-N(1)-C(5)	155.45(1)	157.58(0)	155.37(7)	155.71(5)
N(1)-C(5)-C(1)	178.31(5)	178.71(3)	177.49(2)	178.58(1)
Cp-pyrazole twist angle	-14.93	8.74	-11.17	-13.16
N(2)-N(1)-C(4)-C(5) ϕ_1	-45.37	46.92	-42.92	-42.75
C(7)-N(1)-C(4)-C(3) ϕ_2	-38.22	51.47	-33.56	-34.06

Electrochemical Studies

Electrochemical potentials for second order NLO chromophores provide required information about HOMO and LUMO energy levels.[30] Therefore, we have carried out cyclic voltammetry (CV) measurements at 0.2 Vs^{-1} on a glassy carbon working electrode in acetonitrile

solution with 0.1 M tetrabutylammonium perchlorate (TBAP) as the supporting electrolyte. A saturated calomel electrode (SCE) was used as the operating reference electrode and a platinum wire as the counter electrode. The electrochemical data of the oxidation and reduction processes of the chromophores **1, 7-12** are reported in Table 2, and the representative cyclic voltammograms of **8, 9** and **10** are shown in Figure S10. All the chromophores display the first oxidation peak reversible or quasi-reversible from both the electrochemical and chemical point of view with a current ratio (i_{pa}/i_{pc}) equal to unity, assignable to the monoelectronic oxidation process of the ferrocenyl ($Fe^{II} \leftrightarrow Fe^{III}$) moiety within the potential range of +0.44 to +0.36 V. Compared to 0.40 V of the oxidation potential of the free ferrocene in the same experimental conditions,[31] the chromophores **8, 9** and **10** exhibit slightly higher oxidation potentials, while the chromophores **1, 7, 11** and **12** show slightly lower potentials.[32]

However, the peak corresponding to the reduction could be detected only for chromophores **8, 9, 10** (Table 2 and Figure S10), carrying electron withdrawing groups in a *para* position of the aryl ring. The reduction peak, which corresponds to a monoelectronic process centered on the aromatic moiety of the chromophores **1, 7, 11** and **12**, was not detected in the working potential window. This can be explained by the significant effect produced on the reduction potential by the electron withdrawing properties of the substituent in the *para* position. In fact the potential of the reduction process shifts significantly from -1.79 V (**8**) to -2.17 V (**9**) and -2.39 V (**10**) as expected for a more easy process by increasing the electron withdrawing properties of the substituent in the *para* position of the aromatic ring.

Therefore, it appears that the potential of the oxidation process, which is centered on the ferrocenyl moiety, is only slightly affected by the electronic effects induced by the substituent, while the potential of the reduction process, which is centered on the aromatic ring, is significantly affected. It follows that the energy of electrochemical HOMO level is quite comparable for all the chromophores while the energy of the electrochemical LUMO level is higher for **9** and **10** when

compared to **8** and probably much higher for **1, 7** and particularly for **11** and **12**. Any attempt to evaluate the energy of the LUMO levels of **1, 7, 11** and **12** by the electrochemical and optical method ($E_{LUMO}= E_{HOMO} + E_g^{optical}$ where $E_g^{optical}= 1239.84187/\lambda_{onset}$) failed, due to the very weak intensity and broad characteristic of their low-energy absorption band, which introduces a great difficulty in defining the value of λ_{onset} without introducing large errors.

Table 2. Key CV features of chromophores **1**, **7-12** and electrochemical energy levels HOMO and LUMO derived therefrom.

Chromophore	$E_{1/2,Ic}$ **[V]**	$E_{1/2,Ia}$ **[V]**	E_{LUMO} **[eV]**[b]	E_{HOMO} **[eV]**[c]	$E_{HOMO-LUMO}$ **[eV]**
1	n.d.	0.38	n.d.	-4.78	n.d.
7	n.d.	0.37	n.d.	-4.77	n.d.
8[a]	-1.79	0.41	-2.66	-4.81	2.16
9	-2.17	0.44	-2.23	-4.84	2.61
10	-2.39	0.44	-2.01	-4.84	2.83
11	n.d.	0.36	n.d.	-4.76	n.d.
12	n.d.	0.37	n.d.	-4.77	n.d.

a) A reduction peak is detected at -1.05 V, corresponding to the reduction of the nitro group (see Figure S10) b) $E_{LUMO} = -(E_{1/2,Ic} + 4.4)$ c) $E_{HOMO} = -(E_{1/2,Ia} + 4.4)$ (n.d.= not detected).

Electronic absorption spectra

The absorption spectra of the chromophores **1** and **7-12** in CH_3CN solution are shown in Figure 4a, and HE (high energy), ME (medium energy) and LE (low energy) absorption bands of chromophores **9** and **10** in Figure 4b, while detailed data about the absorption maxima of chromophores **1** and **7-12** are reported in Table 3. All the chromophores depict an intense absorption band in the range 264-320 nm (HE), and a less intense band which sometimes, as in the case of **8, 11** and **12** is a barely distinguishable shoulder in the region 335-380 nm (ME). Finally, all the chromophores show a very weak absorption band at about 440-460 nm (LE) only slightly dependent upon the nature of the substituent in the *para* position of the aryl ring (Table 3).

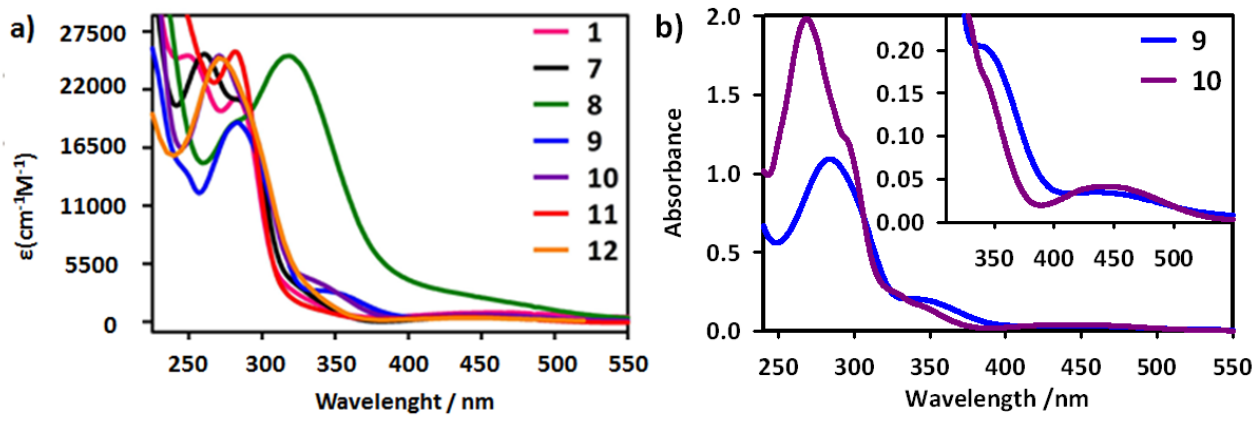

Figure 4. a) Electronic absorption spectra of chromophores **1** and **7-12**. b) HE, ME and LE absorption bands of **9** and **10** in CH_3CN solution.

The HE band can be originated mainly from the N-arylpyrazolic moiety of the chromophores; for instance such very strong absorption band was reported for various N-arylpyrazoles by Miller *et al.*[18] The maximum of the HE band for all the chromophores investigated in this work, with the exception of **8**, is shifted to lower wavelengths with respect to the strong absorption band above 310 nm reported for various N-arylpyrazoles.[18] In agreement with such assignment for 3,5 dimethyl 1-(4-nitrophenyl)-1H pyrazole a strong band with λ_{max} at 311 nm and ε= 11748 M^{-1} cm^{-1} was reported by D.M. Burness.[33]

Table 3. Experimental data of the HE, ME and LE absorption bands of **1**, **7-12** in CH_3CN solution.

Chromophore	**λ_{max}^{HE} [nm (eV)]/ε (×10³) [M^{-1} cm^{-1}]**	**λ_{max}^{ME} [nm (eV)]/ε (×10³) [M^{-1} cm^{-1}]**	**λ_{max}^{LE} [nm (eV)]/ε (×10³) [M^{-1} cm^{-1}]**
1	276 (4.48) /21.5	335(3.70)/1.85	449(2.76)/0.81
7	275 (4.50) /22.9	334(3.71)/2.61	440(2.81)/0.43
8	318 (3.89) /24.8	382(3.24)/6.40[a]	460(2.69)/1.71[a]
9	285 (4.36) /18.3	351(3.53)/2.79	450(2.75)/0.42
10	264 (4.69) /24.5	343(3.61)/3.32	446(2.77)/0.61
11	276 (4.49) /25.2	335(3.70)/1.27[a]	440(2.81)/0.43
12	270 (4.59) /25.1	337(3.67)/2.13[a]	445(2.78)/0.41

a) Barely distinguishable shoulder

The HE band of chromophores **1, 7-12**, like the strong absorption band reported for various N-arylpyrazoles,[18] is not significantly solvatochromic, while its energy is controlled by the nature of the substituent with a strong or significant bathochromic shift for chromophores **8** and **9** carrying stronger electron acceptor groups in para position of the aromatic ring. Taking as reference chromophore **1** the HE band of **8** is red shifted by 42 nm while that of **9** by 9 nm, in agreement with the increased electron withdrawing character of the NO_2 group when compared to the CN group. Conversely, chromophores **11** and **12**, carrying respectively the slightly donor group OCH_3 and the strong donor group NMe_2, show a very small or null hypsochromic shift when compared to **1** (Table 3). It appears thus that the electronic effects produced by the substituents in the *para* position of the aromatic ring are transmitted along the entire molecular skeleton, although the π ferrocenylpyrazolic moiety is not coplanar with the aromatic ring.

This statement is supported by the evidence that 3-ferrocenyl-5-methyl-1H-pyrazole, lacking the aryl ring, shows a strong absorption band in CH_3CN solution at 270 nm (ε = 32125 $M^{-1}cm^{-1}$), blue-shifted with respect to the HE band of all the other chromophores here investigated, with the exception of **12**, (Table 3), whose energy is clearly affected by an ICT process from the donor ferrocenyl pyrazole moiety to the aromatic ring. The ME and LE absorption bands for substituted ferrocene molecules seem to be originated mainly by the ferrocenyl moiety since substituted ferrocenyl molecules are characterized by three absorption bands.[34] The one at a shortest wavelength in the range of 269-289 nm of medium intensity (ε about 3000 $M^{-1}cm^{-1}$), is probably part of the strong HE band of **1, 7-12**. A second weak band (ε about 1200-1800 $M^{-1}cm^{-1}$) in the range 319-335 nm was attributed to an MLCT originated by a n→π* transition from Fe^{II} atom to the cyclopentadienyl ring. A third very weak band at about 440 nm (ε around 460-590 $M^{-1}cm^{-1}$) was assigned to a d-d transition within the d^6 iron atom since it is not dependent on the solvent.

Therefore, the ME band for the chromophores **1, 7-12** (in the range 335-382 nm) can be mainly attributed to an MLCT transition centered on the ferrocenyl π system, perturbed as intensity

and wavelength of the maximum by its coupling with the N-arylpyrazole. In fact, the ME band shows a significant red shift particularly for **8, 9, 10** and an increase in its intensity, (Table 3) with respect to that of the 3-ferrocenyl-5-methyl-1-H-pyrazole (λ_{max} at 335 nm with ε= 1400), lacking the aryl ring.

It appears thus that despite the lack of planarity of the structure of chromophores **1, 7-12** a significant electronic effect is transmitted on the energy and intensity of the MLCT transition of the ferrocenyl moiety according to the electronic nature of the substituent. For instance when comparing chromophore **1** with **8** and **9**, carrying the electron withdrawing groups NO_2 and CN in para position of the aryl ring, the ME band shows a bathochromic shift of 47 nm for **8** and 16 nm for **9** (Table 3), as expected if the ferrocenyl moiety, when linked to an N-arylpyrazole, significantly participates to an ICT process.

Finally, the LE band of chromophores investigated in this work is not solvatochromic and very slightly perturbed as energy by the nature of the substituent, with an exception for **8**, carrying the strong electron withdrawing NO_2 group (Table 3). Such evidence suggests the assignment of this band to a d-d transition centered mainly on the ferrocenyl moiety, not much perturbed by the coupling between the cyclopentadienyl ring and the N-arylpyrazole. In conclusion, the electronic absorption spectra of the chromophores support an ICT process despite the lack of planarity of their structures.

DFT and TD-DFT calculations

In order to find a solid theoretical support to the electronic origin of the ICT process, and consequently the main features of the electronic absorption spectra and of the second order NLO response, B3LYP/6-31+G** and TD (B3LYP/6-31+G**) calculations both in gas phase and in solvent (CH_3CN) phase were carried out for chromophores **1** and **7-12.** The DFT optimized molecular structures of **1** and **7-12**, reported in the Supplementary Information (Figure S10), are

totally in agreement with the main features of the structures deduced from the X- ray crystallographic investigation of **5, 7, 8** and **9**. As it can be deduced from the isodensity plots of Figure 5, reporting also the energy of the HOMO and LUMO levels of **1, 7-12**, the energy of the HOMO level, in agreement with the electrochemical investigation, is not too much influenced by the nature of the substituent in para position of the aromatic ring since the electronic density in the ground state is mainly localized on the ferrocenyl moiety. On the contrary, the energy of the LUMO level is strongly influenced by the substituent, as supported by the electrochemical investigation in the case of **8, 9** and **10**, being the LUMO principally localized on the aromatic ring.

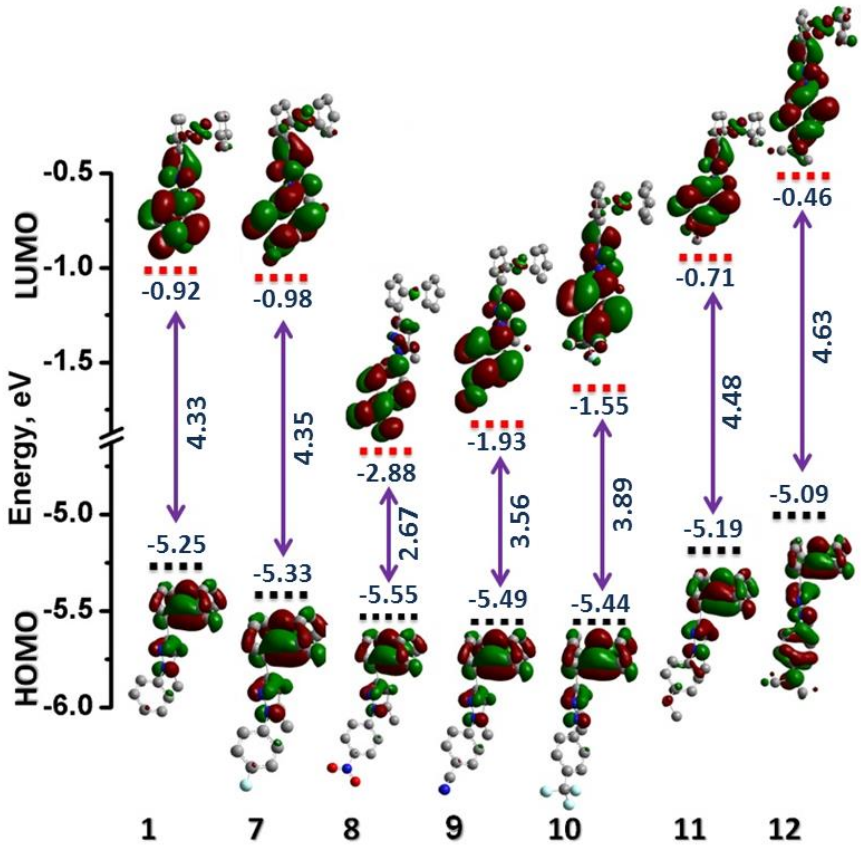

Figure 5. Isodensity plots, energy of the HOMO and LUMO levels and the HOMO-LUMO energy gap of chromophores **1** and **7-12** calculated at the B3LYP/6-31+G** level of theory.

Only in the case of **12**, carrying a strong donor NMe_2 group in a *para* position of the aromatic ring, the HOMO has partially delocalized also on the aromatic ring and the LUMO on the ferrocenyl moiety. In detail the energy of the HOMO level shows, in agreement with the

electrochemical trend, only a slight energy stabilization for **7**, **8, 9** and **10**, and a slight destabilization for **11** and **12,** when compared to **1** (Figure 5). DFT calculated values of the HOMO energy levels, ranging from about -5 to -5.5 eV, are lower than those deduced from the oxidation peaks of the electrochemical investigation (compare Figure 5 and Table 2), which are at about -4.75/-4.85 eV.

The energy of the LUMO level shows, when compared to **1**, a strong stabilization for **8,** carrying the strong electron withdrawing NO_2 group and a significant stabilization for **9** and **10,** carrying less strong electron acceptor groups, while a significant destabilization occurs for **11** and **12** carrying the electron donor OCH_3 and NMe_2 groups. Such trend reproduces quite well that deduced from the electrochemical investigation for **8, 9** and **10** (Table 2). As found for the HOMO levels, the LUMO energy levels, with the exception of **8**, are higher than those deduced from the electrochemical investigation. As a result higher energy gaps are obtained with respect to the electrochemical values (compare Figure 5 and Table 2) though the computed trend properly reproduces the experimental one. In particular for chromophores **8-10**, carrying electron withdrawing groups on the aromatic ring, the DFT calculated HOMO-LUMO energy gap increases from 2.67 eV to 3.56 and 3.89 eV respectively, while the electrochemical energy gap goes from 2.16 eV to 2.61 and 2.83 eV respectively. The disagreement between computed and experimental values can be ascribed on one side to the adopted computational approach and, on the other side, to the effects of solvation and ionic couples which affect the electrochemical values of both the HOMO and LUMO energy levels.

By looking at the frontier orbital distributions of Figure 5, it turns out that the HOMO-LUMO transition corresponds, for **1, 7-11**, to a large transfer of electron density from the ferrocenyl moiety to the N-arylpyrazolic system and particularly to the aromatic ring, while such electron transfer is not so significant for **12**. The role of the pyrazolic part of the molecule is not only that of

allowing the transfer of the electronic density from the ferrocenyl to the aromatic ring but also of electron donor by a partial transfer of its electronic density to the aromatic ring.

We have then made TD-DFT calculations on chromophores **1** and **7-12** to give a definite assignment of the transitions experimentally observed (Table 4). They have confirmed the significant experimental red shift of the HE band by increasing the electron acceptor properties of the substituent in the *para* position of the aromatic ring and the ICT character of such band. A quite satisfactory agreement between calculated (Table 4) and experimental (Table 3) values of λ_{max} of the HE band was found for **1** and **7, 11** and **12**, while for chromophores **9, 10** and particularly **8**, carrying strong electron acceptor groups, the difference between calculated and experimental values of λ_{max} of the HE band is relevant.

The anomaly of chromophore **8** is confirmed by the definition of the various relevant components of the HE band. While for **7, 9, 10, 11** the major component is the HOMO-2 → LUMO transition, for **8** it is the HOMO-2→LUMO+5. It appears that when the substituent can interact by conjugation with the π system of the aromatic ring like in **8** (Figure S10), but also in **12** carrying the strong donor NMe_2 group in the aryl ring (HOMO→LUMO+1 as the major component) there is an effect on the energy levels strongly involving the substituent by conjugation.

Table 4. TD-DFT calculated λ_{max}, *f* and energy contribution to the HE band at the major B3LYP/6-31+G** level of theory for **1**, **7-12**

Chromophore	**TD-DFT calculated λ_{max} and main features of the various relevant components to the HE band**			
	λ_{max}, nm[a]	*f*[a]	Energy, eV[a]	main transition (weight)[b]
1	280 (280)	0.19 (0.42)	4.43 (4.42)	HOMO-5 →LUMO (50%)
7	278 (279)	0.26 (0.41)	4.45 (4.44)	HOMO-2→LUMO (+62%)
8	404 (449)	0.20 (0.25)	3.07 (2.76)	HOMO-2→LUMO+5 (68%)
9	322 (329)	0.36 (0.46)	3.85 (3.76)	HOMO-2→LUMO (+100%)
10	301 (301)	0.31 (0.41)	4.11 (4.11)	HOMO-2→LUMO (+100%)
11	277 (278)	0.30 (0.46)	4.47 (4.45)	HOMO-2→LUMO (+62%)
12	295 (299)	0.29 (0.38)	4.19 (4.14)	HOMO→LUMO+1 (+44%)

a) Values in parentheses are calculated in CH_3CN solution. b) only components with contribution greater than 44% are shown. Percentage contribution approximated by $2\times(c_i)^2\times100\%$, where c_i is the coefficient for the particular orbital rotation.

Interestingly it turns out that the HE band, attributable mainly to the HOMO-2→LUMO transition for **7** and **9-11**, and corresponding to a large transfer of electron density from the ferrocenylpyrazolic system to the aromatic ring, involves a significant ICT process (Figure 6 left). On the other hand in chromophore **12** the major contribution to the HE band is the HOMO→LUMO+1 transition (Table 4), associated with a much less significant transfer of electronic density from the ferrocenyl and partially the pyrazolic system to the aromatic ring where the substituent is a strong electron donor, so as to prevent the ICT process (Figure 6 right).

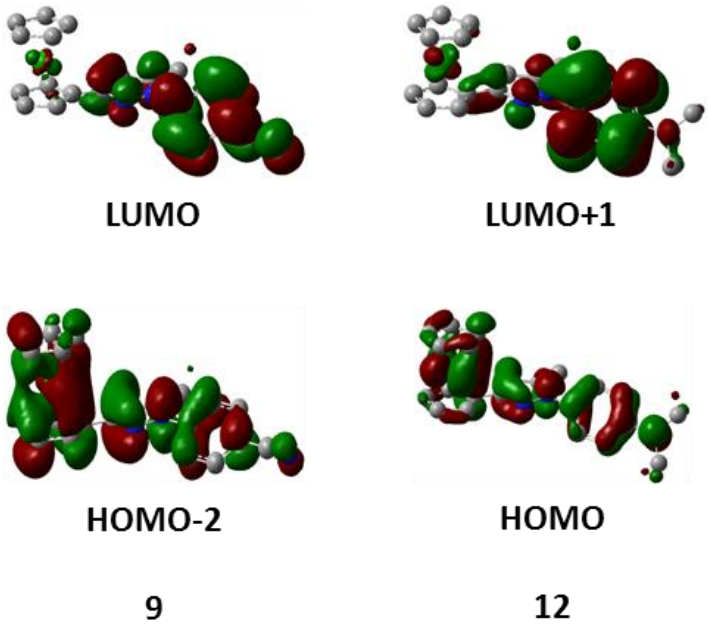

Figure 6. Isodensity plots of HOMO-2→LUMO and HOMO→LUMO+1 transitions mainly involved in the HE absorption band of chromophores **9** and **12** respectively calculated by the TD-DFT approach at B3LYP/6-31+G** level.

Second-order Nonlinear Optical Properties

The second order NLO responses of the molecular chromophores **1** and **7-12** were measured by the EFISH technique, which provides the γ_{EFISH} value, from which EFISH quadratic hyperpolarizability β_λ can be obtained through eq. 1

$$\gamma_{EFISH} = (\mu\beta_\lambda / 5KT) + \gamma(-2\omega;\omega,\omega,0) \quad (1)$$

where μ is the ground state dipole moment, $\mu\beta_\lambda$/5kT the dipolar orientational contribution, λ is the fundamental wavelength of the incident photons in the EFISH experiment, γ(-2ω;ω, ω, 0) is a third-order term at frequency ω of the incident photons, corresponding to the cubic contribution to γ_{EFISH}, usually negligible for quite dipolar chromophores such as those studied in this work. Finally, β_λ is the projection along the dipole moment axis of the vectorial component β_{VEC} of the tensorial quadratic hyperpolarizability. In the following β_λ is reported as β_{1907} since the EFISH experiments were carried out working with a 1907 nm non-resonant incident wavelength. All the EFISH measurements were carried out in $CHCl_3$ solutions at 10^{-3} M concentration (see experimental). The experimental $\mu\beta_{1907}$ values obtained for chromophores **1**, and **7-11** (each experimental value is the averages of 16 measurements) are reported in Table 5B, while the theoretical DFT values of the ground (μ_g) and first excited state (μ_e) dipole moments, together with the theoretical β and $\mu\beta$ values calculated by the TD-DFT approach are reported in Table 5A. The $\mu\beta_{1907}$ value of chromophore **12** was too small to be measured by the EFISH technique.

The experimental EFISH $\mu\beta_{1907}$ value and, according to the two-level approximation,[35] the theoretical quadratic hyperpolarizability β are positive for all the chromophores, being DFT calculated $\Delta\mu$ values always positive and dependent upon the nature of the substituents in the *para* position of the aryl ring (Tables 5A and 5B), as expected for a ICT process involving a transfer of electronic density from the donor ferrocenyl pyrazole moiety to the aromatic ring (Figure 6) with an increase of the excited state dipole moment with respect to the ground state.

It turns out that according to the electron withdrawing strength of the substituent, β values between 7 and 91 x 10^{-30} esu have been calculated for chromophores **1** and **7-12**, with the higher values corresponding to **8,** carrying the NO_2 group, to **9,** carrying the CN group, and to **10,** carrying the CF_3 group, all with high or significant electron withdrawing properties (Table 5A). The calculated values of β and $\mu\beta$ of **8** are anomalously high if compared to the other chromophores (Table 5A), but in line with the anomalously high redshift of its HE absorption band and with the much lower HOMO-LUMO gap. Evidence that the β value of chromophores **1** and **7-11** is dominated by an ICT process, involving a significant electron transfer from the DD (donor-donor) ferrocenylpyrazole moiety to the acceptor aromatic ring, is confirmed by the very low value calculated for β of the DDD (donor-donor-donor) chromophore **12,** carrying the strong donor dimethylamino group on the aryl ring (Table 5A).

It must be pointed out that theoretical β and $\mu\beta$ values of all the chromophores investigated have been calculated by the TD-DFT approach using the less complete 6-31+G** basis set, and the B3LYP method (see Experimental) which cannot account in a satisfactory way the electron correlation effects. Therefore, although both the B3LYP method and the basis set 6-31+G** cannot produce a satisfactory estimation of β values, they have been utilized in order to save computational time when compared to inclusion of additional diffusion functions, which would require, for each chromophore, the choice of an appropriate basis set for calculating a reliable β value. It follows that, due to the above limitations, the calculated β values can give acceptable information on the general trend (Tables 5A and 5B) for the series of chromophores **1** and **7-12,** but not on the absolute value of β of each chromophore.

Despite this limitation, the expected trend between EFISH $\mu\beta_{1907}$ and the theoretical $\mu\beta$ values can be observed (Table 5A and 5B). We have thus calculated from β_{1907} values, by the two levels approximation,[35] taking as a reference of the energy of the first excited state of the HE band,

static β_0 and consequently $\mu\beta_0$ values corresponding to the zero incident wavelength (Table 5B) which should be better compared to TD-DFT calculated $\mu\beta$ values. We have found thus that absolute values of theoretical $\mu\beta$ and experimental EFISH $\mu\beta_{1907}$ or $\mu\beta_0$ values of the various chromophores display an acceptable correlation, although not enough linear, reproduced in Figure 7.

Table 5A. Theoretical TD-DFT ground and first excited state dipole moments and values of β and $\mu\beta$ for **1**, **7-12**.

Chromophore	μ_g[a] **(D)**	μ_e[b] **(D)**	$\Delta\mu$[c] **(D)**	$\mu\beta \times 10^{-48}$**(esu)**	$\beta \times 10^{-30}$**(esu)**
1	2.88	3.07	0.19	20.4	7.1
7	3.10	3.44	0.34	52.7	17
8	6.77	8.44	1.67	616	91
9	6.15	7.57	1.42	228	37
10	4.42	5.02	0.60	88.4	20
11	3.60	3.93	0.33	43.2	12
12	4.82	5.18	0.36	13.0	2.7

a) μ_g = ground state dipole moment. b) μ_e = excited state dipole moment. c) $\Delta\mu$ = difference between excited and ground state dipole moment.

Table 5B. Experimental EFISH $\mu\beta_{1907}$ and $\mu\beta_0$ for **1**, **7-11**.

Chromophore	μ**(D)**[a]	$\mu\beta_{1907} \times 10^{-48}$ **(esu)**	$\mu\beta_0$[b] $\times 10^{-48}$ **(esu)**
1	2.88	280	251
7	3.10	335	301
8	6.77	410	355
9	6.15	360	320
10	4.42	330	299
11	3.60	320	287
12	4.82	n.d.[c]	n.d.[c]

a) Theoretical DFT value of the ground state μ_g; b) static value calculated applying the two level approximation[35] to EFISH β_{1907} taking as reference the energy of the first excited state of the HE band; c) too low value to be measured with an acceptable error.

Although such lack of linearity, mainly due to anomalously high $\mu\beta_{1907}$ and $\mu\beta$ values of **8,** it appears that the trend of the second order NLO response, experimentally measured as $\mu\beta_{1907}$ or theoretical as $\mu\beta$ is related, in a satisfactory way, to the σ values of the Hammet parameters[36] of the substituents in para position of the aryl ring, which according to Ulman take into account both

inductive and resonance effects.[37] In agreement with the larger red shift of both HE and ME electronic absorption bands of **8** and **9** with respect to **1**, due to a more significant ICT process, both theoretical $\mu\beta$ and experimental $\mu\beta_{1907}$ values are much higher for **8** and **9**, carrying stronger electron withdrawing groups with respect to other chromophores (Tables 5A and 5B)

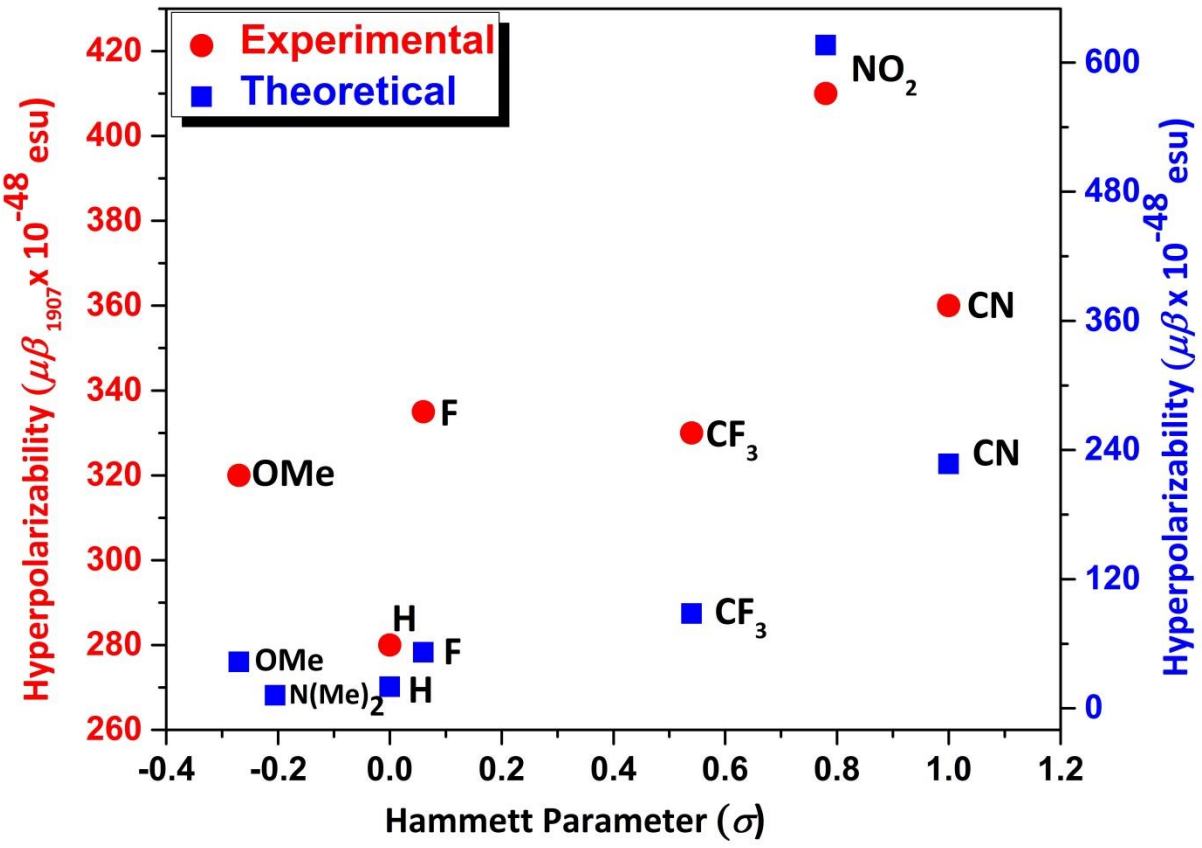

Figure 7. Correlation of the general trend of theoretical $\mu\beta$ and experimental EFISH $\mu\beta_{1907}$ values for chromophores **1** and **7-12** and their relation with respect to the electronic properties of substituents in para position of the aryl ring as defined by the Hammett parameters (σ).[36]

Finally, it is of interest to compare the magnitude of static β_0 values of **1, 7-11,** not dependent on the wavelength of the incident light, with static β_0 values reported by Miller et al.[18] for a series of structurally related DA (donor-acceptor) ICT chromophores based on various N-arylpyrazoles, lacking the ferrocenyl moiety. In accordance with a more significant ICT process, DDA (donor-donor-acceptor) chromophores **1, 7-11**, based on the ferrocenyl N-aryl pyrazole structure, show β_0 values between 52.1 and 97.1 x 10^{-30} esu, much higher than those of the series of

the structurally related DA chromophores, reported by Miller *et al*.,[18] which show β_0 values between 4.6 and 30.7 x 10^{-30} esu.

Conclusions

In this paper, we report on a series of new DDA chromophores based on the ferrocenyl N-aryl pyrazolic structure successfully synthesized using the Chan-Lam cross-coupling reaction between the appropriate arylboronic acid and the ferrocenyl pyrazole moiety. The chromophores **5, 7**, **8** and **9**, fully characterized by single crystal X-ray diffraction, show a non-planar structure with a slight twist angle between the cyclopentadienyl ring of the ferrocenyl and the pyrazolic moieties with significant torsion angles between the DD donor ferrocenyl pyrazole and the aryl ring. Such structures have been confirmed by DFT calculations for all the chromophores.

Electronic absorption spectra and TD-DFT theoretical investigation have produced evidence for a significant ICT process from the ferrocenyl system to the aryl ring. Despite the lack of planarity, we have found that the effects induced by the electronic properties of the substituents in the *para* position of the aryl ring are transmitted along the molecular structure to the ferrocenyl pyrazolic moiety acting as DD strong donor while the aryl ring acts as the acceptor part of the ICT process. It follows that the features of electronic absorption spectra, electrochemical measurements and second order NLO responses of these new ICT chromophores are significantly tuned by the nature of the substituents in the *para* position of the aryl ring.

The second order NLO responses, theoretically evaluated as the $\mu\beta$ value calculated by the TD-DFT method or experimentally measured as $\mu\beta_{1907}$ by the EFISH technique, working with a 1907 nm non-resonant incident wavelength, increase with increasing the strength of the acceptor properties of the substituents, with anomalously high values in the case of the NO_2 group, so that the correlation between the trend of theoretical $\mu\beta$ and experimental EFISH $\mu\beta_{1907}$ values is not linear enough, although the relation of both $\mu\beta$ and $\mu\beta_{1907}$ values with the Hammet σ parameters of the various substituents is quite satisfactory.

The static β_0 values of the DDA ferrocenyl N-arylpyrazole chromophores investigated in this work, calculated by the two levels approximation taking as reference the energy of the first excited state of the HE absorption band, are much higher (between 52.1 and 97.1 x 10^{-30} esu) than the β_0 values reported by Miller et al.[18] for the structurally related DA, N-arylpyrazoles lacking of the donor ferrocenyl moiety (between 4.6 and 30.7 x 10^{-30} esu), thus confirming both the high donor properties of the ferrocenyl moiety and that the connection of two strong donor moieties can induce a strong increase of the second order NLO response of an ICT chromophore. Finally, the $\mu\beta_0$ values of all the chromophores investigated in this work are unexpectedly relevant (between 251 and 355 x 10^{-48} esu), taking into consideration the lack of planarity of the π system of their structures.

In conclusion by the investigation of the NLO properties of these new ICT chromophores based on ferrocenyl N-arylpyrazolic structures we have shown that even in the presence of a relatively low planarity of the whole π structure, the second order NLO response can be significantly tuned by the nature of the substituent on the aryl ring and that the introduction of a strong donor as the ferrocenyl moiety in the N-arylpyrazolic structure, producing a DDA structural arrangement, is the origin of a large increase of the second order nonlinear response. Moreover TD-DFT calculations clearly show that the pyrazolic part of the molecule does not act as a simple π spacer between the donor ferrocenyl moiety and the acceptor aryl ring, as it occurs in classical push-pull systems, but mainly as an additional π donor, which strengthens the donor properties of the ferrocenyl thus favoring a very effective ICT process by a DDA system.

It follows that the experimental and theoretical investigation reported in this work might provide better insight for devising a wide variety of new chromophoric DDA structures not planar with extensive electron transfer along the molecular skeleton, and interesting second order nonlinear optical properties due to a significant ICT process.

Experimental

Materials and Synthetic Procedures

The 3-Ferrocenyl-5-methyl-1H-pyrazole was synthesized according to the reported procedure.[22] Chromatographic purifications and separations were carried out using silica gel 60 (AVRA, 100 − 120 mesh). CH_2Cl_2 was distilled over $CaCl_2$ prior to use. Other solvents were of reagent grade and were used without prior purification. All other chemicals were purchased from M/s. Aldrich Chemical Co. and M/s.Johnson Matthey Chemicals. Details on the general experimental conditions and on the analytical characterisation of chromophores are reported in the Supporting Information.

General Physical Measurements

The ^{1}NMR spectra were recorded on a BRUKER (600 MHz) spectrometer. Chemical shifts are reported in δ (ppm) and mass spectra were recorded on a GC-MS (PERKIN ELMER) spectrometer Infrared spectra were recorded on a PERKIN SHIMADZU spectrometer spectrum One as KBr diluted discs. Electronic absorption spectra were recorded using Agilent 8453 UV-visible diode array spectrophotometer in CH_3CN as a solvent. Electrochemical measurements were performed in a 4 cm^3 cell, in 5×10^{-4} - 10^{-3} M solutions in acetonitrile (Aldrich, 99.8%) with 0.1 M tetrabutylammonium perchlorate (TBAP, Aldrich) as the supporting electrolyte. The solutions were de-aerated by N_2 bubbling. The ohmic drop has been compensated by the positive feedback technique. The experiments were carried out using an AUTOLAB PGSTAT potentiostat (EcoChemie, The Netherlands) run by a PC with GPES software. Cyclic voltammetry (CV) investigations were carried out at scan rates typically ranging 0.05 to 2 Vs^{-1}, with ohmic drop compensation. The working electrode was a glassy carbon one (AMEL, diameter = 1.5 mm) cleaned by synthetic diamond powder (Aldrich, diameter = 1 μm) with a wet cloth (STRUERS DP-NAP); the counter electrode was a platinum wire. The operating reference electrode was an aqueous

saturated calomel electrode (SCE). To prevent water and chloride leakage into the working solution a compartment filled with the operating medium and ending with a porous frit was interposed between the reference electrode and the cell. Thermogravimetric analyses (TGA) were performed (0-1000 ˚C) on a TGA SDT Q600 V20.9 Build 20 instrument under N_2 atmosphere, at a heating rate of 20 ˚C min^{-1}.

Single-crystal X-ray structural determination of chromophores 5, 7-9

Crystals of **5, 7-9** were obtained by a slow evaporation of the solutions (MeOH and DCM) at room temperature. Crystals were stored in paraffin oil, mounted in a MiTeGenloop, and X-ray diffraction measurements were done in the range 100 to 120 K. The crystal approximate dimensions are 0.37 x 0.25 x 0.09 mm^3 (**5**), 0.35 x 0.23 x 0.17 mm^3 (**7**), 0.45 x 0.18 x 0.08 mm^3 (**8**) and 0.35 x 0.27 x 0.21 mm^3 (**9**). The X-ray diffraction data were collected on an Agilent SuperNova (Oxford Diffraction) diffractometer using Mo-K_α radiation (λ = 0.71073 Å). The Apex2[38] package was used for cell refinements and data reductions. The structures were solved by direct methods using the Shelxs 97[39] or Superflip[40] program with the Olex 2[41] graphical user interface. Structural refinements were carried out using Shelxl-97 or Shelxl-2014.[40,42]

The positions of all the atoms were obtained by direct methods. All non-hydrogen atoms were refined anisotropically. Hydrogen atoms were positioned geometrically and were also constrained to ride on their parent atoms, with C − H = 0.95 − 0.1.00 Å, and U_{iso} = 1.2 − 1.5U_{eq} (parent atom). The crystallographic details are summarized in Table S1.

EFISH measurements

All of the EFISH measurements[43] were carried out in $CHCl_3$ solutions at 10^{-3} M concentration, working with a nonresonant incident wavelength of 1907 nm, using a Q-switched, mode-locked Nd^{3+}:YAG laser [pulse durations of 15 ns (90 ns) at a 10 Hz repetition rate] manufactured by Atalaser. The 1064 nm initial wavelength was shifted to 1907 nm by a Raman

shifter with a high-pressure H_2 cell. The apparatus for the EFISH measurements was made by SOPRA (France).

A high voltage was applied across the EFISH cell containing the solution. The EFISH cell consisted of a stainless steel container with two quartz optical windows that form a wedge-shaped cavity within the cell. The electrode was connected to the high voltage supply. The cell was mounted on an electrically isolated translation stage. The whole cell was then translated horizontally relative to the incident beam to produce fringes at the second harmonic wavelength. Every measurement was referenced separately to the fringes of the pure solvent ($CHCl_3$) that was used to dissolve the chromophore to consider laser power's fluctuations. The $\mu\beta_{1907}$ values reported in Table 5B are the averages of 16 successive measurements performed on each sample. The standard deviation was never greater than 20%.

Theoretical Calculations

The electronic structures and molecular properties oft he ferrocenyl-N-pyrazolic chromophores investigated in this work were studied using the DFT (Density Functional Theory) method in order to define bonding patterns, electronic charge, and molecular orbital energy distributions, and the TD (Time Dependent)-DFT method to investigate the origin of electronic absorption spectra and nonlinear optical properties. The initial geometry of chromophores was taken from the available crystal data of **9** and guess structures of remaining chromophores were obtained by changing the substituent in the *para* position of the aryl ring. The geometries of the chromophores **1, 7-12** in the gas phase were optimized using the Becke's three-parameter and Lee-Yang-Parr functional (B3LYP).[44] The DFT calculations were carried out using the 6-31+G** basis set. On the optimized gas phase geometries, TD-DFT single point calculations have been carried out at the B3LYP/6-31+G** level, including the first 20 excited singlet states, both in the gas phase and insolvent (CH_3CN) phase using PCM (Polarizable Continuum Model) as solvation method. All

calculations were performed using the G09 package.[45] Electronic isodensity plots of frontier molecular orbitals were obtained using GaussView 5[46] molecular visualization program.

Acknowledgements

KSK thanks to DST for Inspire fellowship (IF-110138). KSK and NP gratefully acknowledge SIF DST-VIT-FIST, VIT University, Vellore for providing NMR, Mass and IR data. MP thanks, Prof. Renato Ugo, Prof. Patrizia Mussini and Dr. Alessandra Forni for their extremely useful suggestions and comments.

Keywords: Ferrocenyl-N-arylpyrazole, N-arylation, Chan-Lam Coupling, Nonlinear optics, EFISH

Supporting Information

X-ray crystallographic data (1421536-1421538 (**5**, **7**, **9**) and 1428469 (**8**)) in CIF format and CIF check and Cartesian coordinates, NMR, Mass, Cyclic Voltagram data. This material is available free of charge via the Internet at http://pubs.acs.org.

Author Information

Corresponding Authors

*E-mail: palanisami.n@gmail.com, maddalena.pizzotti@unimi.it

Notes

The authors declare no competing financial interest.

References

(1) (a) Allard, S.; Forster, M.; Souharce, B.; Thiem, H.; Scherf, U. Organic Semiconductors for Solution-Processable Field-Effect Transistors (OFETs). *Angew. Chem. Int. Ed.* **2008**, *47* (22), 4070–4098; (b) Heck, J.; Dabek, S.; Meyer-Friedrichsen, T.; Wong, H. Mono- and Dinuclear Sesquifulvalene Complexes, Organometallic Materials with Large Nonlinear Optical Properties. *Coord. Chem. Rev.* **1999**, *190-192*, 1217–1254; (c) Clifford, J. N.; Martínez-

Ferrero, E.; Viterisi, A.; Palomares, E. Sensitizer Molecular Structure-Device Efficiency Relationship in Dye Sensitized Solar Cells. *Chem. Soc. Rev.* **2011**, *40* (3), 1635–1646; (d) Wu, Y.; Zhu, W. Organic Sensitizers from D-π-A to D-A-π-A: Effect of the Internal Electron-Withdrawing Units on Molecular Absorption, Energy Levels and Photovoltaic Performances. *Chem. Soc. Rev.* **2013**, *42* (5), 2039–2058.

(2) (a) Joseph W. Perry. *Materials for Nonlinear Optics*; Marder, S. R., Sohn, J. E., Stucky, G. D., Eds.; ACS Symposium Series; American Chemical Society: Washington, DC, 1991; Vol. 455; (b) Twieg, R.; Azema, A.; Jain, K.; Cheng, Y. Y. Organic Materials for Non-Linear Optics Nitropyridine Derivatives. *Chem. Phys. Lett.* **1982**, *92* (2), 208–211; (c) Oudar, J. L.; Hierle, R. An Efficient Organic Crystal for Nonlinear Optics: Methyl- (2,4-Dinitrophenyl) - Aminopropanoate. *J. Appl. Phys.* **1977**, *48* (7), 2699.

(3) (a) Zyss, J.; Ledoux, I. Nonlinear Optics in Multipolar Media: Theory and Experiments. *Chem. Rev.* **1994**, *94* (1), 77–105; (b) Wolff; Siegler; Matschiner; Wortmann. Optimized Two-Dimensional NLO Chromophores with a Threefold Symmetry Axis The Authors Would like to Thank the Volkswagenstiftung and the Fonds Der Chemischen Industrie for Generous Financial Supports of This Work. *Angew. Chem. Int. Ed. Engl.* **2000**, *39* (8), 1436–1439; (c) Verbiest, T.; Clays, K.; Samyn, C.; Wolff, J.; Reinhoudt, D.; Persoons, A. Investigations of the Hyperpolarizability in Organic Molecules from Dipolar to Octopolar Systems. *J. Am. Chem. Soc.* **1994**, *116* (20), 9320–9323; (d) Zyss, J. Molecular Engineering Implications of Rotational Invariance in Quadratic Nonlinear Optics: From Dipolar to Octupolar Molecules and Materials. *J. Chem. Phys.* **1993**, *98* (9), 6583; (e) Ledoux, I.; Zyss, J.; Siegel, J. S.; Brienne, J.; Lehn, J.-M. Second-Harmonic Generation from Non-Dipolar Non-Centrosymmetric Aromatic Charge-Transfer Molecules. *Chem. Phys. Lett.* **1990**, *172* (6), 440–444.

(4) (a) Barlow, S.; Marder, S. R. Electronic and Optical Properties of Conjugated Group 8 Metallocene Derivatives. *Chem. Commun.* **2000**, No. 17, 1555–1562; (b) Blackburn, O. A.; Coe, B. J. Syntheses, Electronic Structures, and Dichroic Behavior of Dinuclear Cyclopalladated Complexes of Push−Pull Azobenzenes. *Organometallics* **2011**, *30* (8), 2212–2222; (c) Blackburn, O. A.; Coe, B. J.; Helliwell, M. Tetrapalladium(II) Bisazobenzene and Azoazoxybenzene Complexes: Syntheses, Electronic Structures, and Optical Properties. *Organometallics* **2011**, *30* (18), 4910–4923; (d) Calabrese, J. C.; Cheng, L. T.; Green, J. C.; Marder, S. R.; Tam, W. Molecular Second-Order Optical Nonlinearities of Metallocenes. *J. Am. Chem. Soc.* **1991**, *113* (19), 7227–7232; (e) Coe, B. J.; Fielden, J.; Foxon, S. P.; Asselberghs, I.; Clays, K.; Van Cleuvenbergen, S.; Brunschwig, B. S. Ferrocenyl Diquat Derivatives: Nonlinear Optical Activity, Multiple Redox States, and Unusual Reactivity. *Organometallics* **2011**, *30* (21), 5731–5743; (f) Coe, B. J.; Houbrechts, S.; Asselberghs, I.; Persoons, A. Efficient, Reversible Redox-Switching of Molecular First Hyperpolarizabilities in Ruthenium(II) Complexes Possessing Large Quadratic Optical Nonlinearities. *Angew. Chem. Int. Ed.* **1999**, *38* (3), 366–369; (g) Green, M. L. H.; Marder, S. R.; Thompson, M. E.; Bandy, J. A.; Bloor, D.; Kolinsky, P. V.; Jones, R. J. Synthesis and Structure of (Cis)-[1-Ferrocenyl-2-(4-Nitrophenyl)ethylene], an Organotransition Metal Compound with a Large Second-Order Optical Nonlinearity. *Nature* **1987**, *330* (6146), 360–362; (h) Ishizuka, T.; Sinks, L. E.; Song, K.; Hung, S.-T.; Nayak, A.; Clays, K.; Therien, M. J. The Roles of Molecular Structure and Effective Optical Symmetry in Evolving Dipolar Chromophoric Building Blocks to Potent Octopolar Nonlinear Optical Chromophores. *J. Am. Chem. Soc.* **2011**, *133* (9), 2884–2896.

(5) Coe, B. J. Developing Iron and Ruthenium Complexes for Potential Nonlinear Optical Applications. *Coord. Chem. Rev.* **2013**, *257* (9-10), 1438–1458.

(6) Bella, S. Di; Dragonetti, C.; Pizzotti, M.; Roberto, D.; Tessore, F.; Ugo, R. *Molecular Organometallic Materials for Optics*; Bozec, H., Guerchais, V., Eds.; Topics in Organometallic Chemistry; Springer Berlin Heidelberg: Berlin, Heidelberg, 2010; Vol. 28.

(7) (a) Woodward, R. B.; Rosenblum, M.; Whiting, M. C. A New Aromatic System. *J. Am. Chem. Soc.* **1952**, *74* (13), 3458–3459; (b) Benkeser, R. A.; Goggin, D.; Schroll, G. A Route to Monosubstituted Ferrocene Compounds. *J. Am. Chem. Soc.* **1954**, *76* (15), 4025–4026; (c) Miller, S. A.; Tebboth, J. A.; Tremaine, J. F. 114. Dicyclopentadienyliron. *J. Chem. Soc.* **1952**, 632.

(8) Barlow, S.; O'Hare, D. Metal−Metal Interactions in Linked Metallocenes. *Chem. Rev.* **1997**, *97* (3), 637–670.

(9) Miller, J. S.; Epstein, A. J. Organic and Organometallic Molecular Magnetic Materials—Designer Magnets. *Angew. Chem. Int. Ed.* **1994**, *33* (4), 385–415.

(10) (a) Imahori, H.; Tamaki, K.; Guldi, D. M.; Luo, C.; Fujitsuka, M.; Ito, O.; Sakata, Y.; Fukuzumi, S. Modulating Charge Separation and Charge Recombination Dynamics in Porphyrin−Fullerene Linked Dyads and Triads: Marcus-Normal versus Inverted Region. *J. Am. Chem. Soc.* **2001**, *123* (11), 2607–2617; (b) Ratera, I.; Sporer, C.; Ruiz-Molina, D.; Ventosa, N.; Baggerman, J.; Brouwer, A. M.; Rovira, C.; Veciana, J. Solvent Tuning from Normal to Inverted Marcus Region of Intramolecular Electron Transfer in Ferrocene-Based Organic Radicals. *J. Am. Chem. Soc.* **2007**, *129* (19), 6117–6129.

(11) Beer, P. D. Transition-Metal Receptor Systems for the Selective Recognition and Sensing of Anionic Guest Species. *Acc. Chem. Res.* **1998**, *31* (2), 71–80.

(12) (a Mata, J. A.; Peris, E.; Asselberghs, I.; Van Boxel, R.; Persoons, A. Large Second-Order NLO Properties of New Conjugated Oligomers with a Pendant Ferrocenyl and an End-Capped Pyridine. *New J. Chem.* **2001**, *25* (8), 1043–1046; (b) Barlow, S.; Bunting, H. E.;

Ringham, C.; Green, J. C.; Bublitz, G. U.; Boxer, S. G.; Perry, J. W.; Marder, S. R. Studies of the Electronic Structure of Metallocene-Based Second-Order Nonlinear Optical Dyes. *J. Am. Chem. Soc.* **1999**, *121* (15), 3715–3723.

(13) (a) Bhat, B. A.; Dhar, K. L.; Puri, S. C.; Saxena, A. K.; Shanmugavel, M.; Qazi, G. N. Synthesis and Biological Evaluation of Chalcones and Their Derived Pyrazoles as Potential Cytotoxic Agents. *Bioorg. Med. Chem. Lett.* **2005**, *15* (12), 3177–3180; (b) Hitz, C. B.; Ewing, J.; Hecht, J. *Introduction to Laser Technology*; John Wiley & Sons, Inc.: Hoboken, NJ, USA, 2012.

(14) Jin, M.; Liang, Y. J.; Lu, R.; Chuai, X. H.; Yi, Z. H.; Zhao, Y.; Zhang, H. J. Synthesis and Properties of Photoluminescence and Electroluminescence of Pyrazoline Derivatives. *Synth. Met.* **2004**, *140* (1), 37–41.

(15) Bian, B.; Ji, S.-J.; Shi, H.-B. Synthesis and Fluorescent Property of Some Novel Bischromophore Compounds Containing Pyrazoline and Naphthalimide Groups. *Dye. Pigment.* **2008**, *76* (2), 348–352.

(16) (a) Szukalski, A.; Sznitko, L.; Cyprych, K.; Miniewicz, A.; Mysliwiec, J. Light Amplification in Derivatives of Pyrazoline-Based Systems. *J. Phys. Chem. C* **2014**, *118* (15), 8102–8110; (b) Mysliwiec, J.; Sznitko, L.; Szukalski, A.; Parafiniuk, K.; Bartkiewicz, S.; Miniewicz, A.; Sahraoui, B.; Rau, I.; Kajzar, F. Amplified Spontaneous Emission of 3-(1,1-Dicyanoethenyl)-1-Phenyl-4,5-Dihydro-1H-Pyrazole Molecule Embedded in Various Polymer Matrices. *Opt. Mater. (Amst).* **2012**, *34* (10), 1725–1728; (c) Cyprych, K.; Sznitko, L.; Morawski, O.; Miniewicz, A.; Rau, I.; Mysliwiec, J. Spontaneous Crystalization and Aggregation of DCNP Pyrazoline-Based Organic Dye as a Way to Tailor Random Lasers. *J. Phys. D. Appl. Phys.* **2015**, *48* (19), 195101.

(17) (a) Barberá, J.; Clays, K.; Giménez, R.; Houbrechts, S.; Persoons, A. A.; Serrano, J. L. Versatile Optical Materials: Fluorescence, Non-Linear Optical and Mesogenic Properties of Selected 2-Pyrazoline Derivatives. *J. Mater. Chem.* **1998**, *8* (8), 1725–1730; (b) Manea, A.-M.; Rau, I.; Tane, A.; Kajzar, F.; Sznitko, L.; Miniewicz, A. Poling Kinetics and Second Order NLO Properties of DCNP Doped PMMA Based Thin Film. *Opt. Mater. (Amst).* **2013**, *36* (1), 69–74; (c) Papagiannouli, I.; Szukalski, a.; Iliopoulos, K.; Mysliwiec, J.; Couris, S.; Sahraoui, B. Pyrazoline Derivatives with a Tailored Third Order Nonlinear Optical Response. *RSC Adv.* **2015**, *5* (60), 48363–48367; (d) Makowska-Janusik, M.; Kajzar, F.; Miniewicz, A.; Mydlova, L.; Rau, I. First Principle Calculations of the Electronic and Vibrational Properties of the 3-(1,1-Dicyanoethenyl)-1-Phenyl-4,5-Dihydro-1H-Pyrazole Molecule. *J. Phys. Chem. A* **2015**, *119* (8), 1347–1358; (e) Mukherjee, S.; Salini, P. S.; Srinivasan, A.; Peruncheralathan, S. AIEE Phenomenon: Tetraaryl vs. Triaryl Pyrazoles. *Chem. Commun.* **2015**, *51* (96), 17148–17151.

(18) Miller, R. D.; Moylan, C. R.; Reiser, O.; Walsh, C. a. Heterocyclic Azole Nonlinear Optical Chromophores. 1. Donor-Acceptor Substituted Pyrazole Derivatives. *Chem. Mater.* **1993**, *5* (14), 625–632.

(19) Dwivedi, Y.; de Boni, L.; Gonçalves, P. J.; Mairink, L. M.; Menegatti, R.; Fonseca, T. L.; Zilio, S. C. Experimental and Theoretical Investigation of Optical Nonlinearities in (Nitrovinyl)-1H-Pyrazole Derivative. *Spectrochim. Acta. A. Mol. Biomol. Spectrosc.* **2013**, *105*, 483–487.

(20) (a) Moylan, C. R.; Twieg, R. J.; Lee, V. Y.; Swanson, S. A.; Betterton, K. M.; Miller, R. D. Nonlinear Optical Chromophores with Large Hyperpolarizabilities and Enhanced Thermal Stabilities. *J. Am. Chem. Soc.* **1993**, *115* (26), 12599–12600; (b) Moylan, C. R.; Miller, R. D.; Twieg, R. J.; Betterton, K. M.; Lee, V. Y.; Matray, T. J.; Nguyen, C. Synthesis and Nonlinear

Optical Properties of Donor-Acceptor Substituted Triaryl Azole Derivatives. *Chem. Mater.* **1993**, *5* (10), 1499–1508.

(21) (b) Lam, P. Y. .; Clark, C. G.; Saubern, S.; Adams, J.; Winters, M. P.; Chan, D. M. .; Combs, A. New Aryl/heteroaryl C-N Bond Cross-Coupling Reactions via Arylboronic Acid/cupric Acetate Arylation. *Tetrahedron Lett.* **1998**, *39* (19), 2941–2944. (b) Chan, D. M. .; Monaco, K. L.; Wang, R.-P.; Winters, M. P. New N- and O-Arylations with Phenylboronic Acids and Cupric Acetate. *Tetrahedron Lett.* **1998**, *39* (19), 2933–2936.

(22) Sergeev, E. E.; Fabinskii, P. V.; Fedorov, V. A.; Korol'kova, I. V.; Kulebakin, V. G. Synthesis and Physicochemical Properties of Crystalline Tris(ferrocenoyl)acetonate Hydrates of Some Rare-Earth Elements. *Russ. J. Coord. Chem.* **2008**, *34* (5), 382–387.

(23) Shi, Y.-C.; Zhu, B.-B.; Sui, C.-X. -Pyrazole. *Acta Crystallogr. Sect. E Struct. Reports Online* **2006**, *62* (9), m2389–m2391.

(24) Wanniarachchi, S.; Liddle, B. J.; Lindeman, S. V.; Gardinier, J. R. Preparation, Properties, and Reactivity of carbonylrhodium(I) Complexes of di(2-Pyrazolylaryl)amido-Pincer Ligands. *J. Organomet. Chem.* **2011**, *696* (23), 3623–3636.

(25) (a) Lambert, C.; Wagener, R.; Klein, J. H.; Grelaud, G.; Moos, M.; Schmiedel, A.; Holzapfel, M.; Bruhn, T. A Photoinduced Mixed-Valence State in an Organic Bis-Triarylamine Mixed-Valence Compound with an Iridium-Metal-Bridge. *Chem. Commun.* **2014**, *50* (77), 11350; (b) Kaddouri, H.; Vicente, V.; Ouali, A.; Ouazzani, F.; Taillefer, M. Copper-Catalyzed Arylation of Nucleophiles by Using Butadienylphosphines as Ligands: Mechanistic Insight. *Angew. Chem. Int. Ed.* **2009**, *48* (2), 333–336.

(26) Chevallier, F.; Halauko, Y. S.; Pecceu, C.; Nassar, I. F.; Dam, T. U.; Roisnel, T.; Matulis, V. E.; Ivashkevich, O. a.; Mongin, F. N-Aryl Pyrazoles: DFT Calculations of CH Acidity and

Deprotonative Metallation Using a Combination of Lithium and Zinc Amides. *Org. Biomol. Chem.* **2011**, *9* (12), 4671.

(27) (a) Coe, B. J.; Docherty, R. J.; Foxon, S. P.; Harper, E. C.; Helliwell, M.; Raftery, J.; Clays, K.; Franz, E.; Brunschwig, B. S. Syntheses and Properties of Salts of Chromophores with Ferrocenyl Electron Donor Groups and Quaternary Nitrogen Acceptors. *Organometallics* **2009**, *28* (24), 6880–6892; (b) Kaur, P.; Kaur, M.; Depotter, G.; Van Cleuvenbergen, S.; Asselberghs, I.; Clays, K.; Singh, K. Thermally Stable Ferrocenyl "push–pull" Chromophores with Tailorable and Switchable Second-Order Non-Linear Optical Response: Synthesis and Structure–property Relationship. *J. Mater. Chem.* **2012**, *22* (21), 10597.

(28) (a) Jacquemin, D.; Femenias, A.; Chermette, H.; André, J.-M.; Perpète, E. A. Second-Order Møller−Plesset Evaluation of the Bond Length Alternation of Several Series of Linear Oligomers. *J. Phys. Chem. A* **2005**, *109* (25), 5734–5741; (b) Dehu, C.; Meyers, F.; Bredas, J. L. Donor-Acceptor Diphenylacetylenes: Geometric Structure, Electronic Structure, and Second-Order Nonlinear Optical Properties. *J. Am. Chem. Soc.* **1993**, *115* (14), 6198–6206.

(29) Venkatraman, S.; Kumar, R.; Sankar, J.; Chandrashekar, T. K.; Sendhil, K.; Vijayan, C.; Kelling, A.; Senge, M. O. Oxasmaragdyrin–Ferrocene and Oxacorrole–Ferrocene Conjugates: Synthesis, Structure, and Nonlinear Optical Properties. *Chem. Eur. J.* **2004**, *10* (6), 1423–1432.

(30) Kaur, S.; Dhoun, S.; Depotter, G.; Kaur, P.; Clays, K.; Singh, K. Synthesis, Linear and Nonlinear Optical Properties of Thermally Stable Ferrocene-Diketopyrrolopyrrole Dyads. *RSC Adv.* **2015**, *5* (103), 84643–84656.

(31) Connelly, N. G.; Geiger, W. E. Chemical Redox Agents for Organometallic Chemistry. *Chem. Rev.* **1996**, *96* (2), 877–910.

(32) Misra, R.; Gautam, P.; Mobin, S. M. Aryl-Substituted Unsymmetrical Benzothiadiazoles: Synthesis, Structure, and Properties. *J. Org. Chem.* **2013**, *78* (24), 12440–12452.

(33) BurnesS, D. M. β-Keto Acetals. I. Synthesis of Pyrazoles and Pyrimidines and the Steric Inhibition of Resonance in 5-Alkyl-1- P -Nitrophenylpyrazoles. *J. Org. Chem.* **1956**, *21* (1), 97–101.

(34) Rabie, U. M. Intra- and Intermolecular Charge Transfer: Twin Themes and Simultaneous Competing Transitions Involving Ferrocenes. *Spectrochim. Acta Part A Mol. Biomol. Spectrosc.* **2009**, *74* (3), 746–752.

(35) (a) Oudar, J. L. Optical Nonlinearities of Conjugated Molecules. Stilbene Derivatives and Highly Polar Aromatic Compounds. *J. Chem. Phys.* **1977**, *67* (2), 446; (b) Oudar, J. L.; Chemla, D. S. Hyperpolarizabilities of the Nitroanilines and Their Relations to the Excited State Dipole Moment. *J. Chem. Phys.* **1977**, *66* (6), 2664.

(36) (a) Park, G.; Cho, B. R. First Hyperpolarizabilities of Triazine derivatives.Ab Initio Studies and Hammett Correlation. *J. Phys. Org. Chem.* **2004**, *17* (3), 169–173.; (b) Park, G.; Cho, B. R. First Hyperpolarizabilities of 1,3,5-Tricyano-2,4,6-Tris(styryl)benzene Derivatives:ab Initio Studies and Hammett Correlation. *J. Phys. Org. Chem.* **2005**, *18* (3), 264–267.

(37) Ulman, A. Calculations of Dipole Moments, Optical Spectra, and Second-Order Hyperpolarizability Coefficients of Some Mono- and Disubstituted Stilbene Models for the Design of Nonlinear Optical Materials. *J. Phys. Chem.* **1988**, *92* (8), 2385–2390.

(38) (a) Bruker, A. X. S. "APEX2-Software Suite for Crystallographic Programs." Bruker AXS Inc., Madison. Bruker AXS, Inc.,: Madison, WI, USA 2009. (b) Bruker AXS, SAINT, Bruker AXS, Inc., Madison, WI, USA. 2009.

(39) Sheldrick, G. M. A Short History of SHELX. *Acta Crystallogr. Sect. A* **2008**, *64* (1), 112–122..

(40) Palatinus, L.; Chapuis, G. SUPERFLIP – a Computer Program for the Solution of Crystal Structures by Charge Flipping in Arbitrary Dimensions. *J. Appl. Crystallogr.* **2007**, *40* (4), 786–790.

(41) Dolomanov, O. V.; Bourhis, L. J.; Gildea, R. J.; Howard, J. a K.; Puschmann, H. OLEX2: A Complete Structure Solution, Refinement and Analysis Program. *J. Appl. Crystallogr.* **2009**, *42* (2), 339–341.

(42) G. M. Sheldrick, SHELXTL, Bruker AXS, Inc., Madison, Wisconsin, USA. 2008.

(43) (a) Ledoux, I.; Zyss, J. Influence of the Molecular Environment in Solution Measurements of the Second-Order Optical Susceptibility for Urea and Derivatives. *Chem. Phys.* **1982**, *73* (1-2), 203–213; (b) Singer, K. D. Measurements of Molecular Second Order Optical Susceptibilities Using Dc Induced Second Harmonic Generation. *J. Chem. Phys.* **1981**, *75* (7), 3572; (c) Nisic, F.; Colombo, A.; Dragonetti, C.; Fontani, M.; Marinotto, D.; Righetto, S.; Roberto, D.; Williams, J. A. G. Highly Efficient Acido-Triggered Reversible Luminescent and Nonlinear Optical Switch Based on 5-π-Delocalized-Donor-1,3-di(2-Pyridyl)benzenes. *J. Mater. Chem. C* **2015**, *3* (28), 7421–7427.

(44) (a) Vosko, S. H.; Wilk, L.; Nusair, M. Accurate Spin-Dependent Electron Liquid Correlation Energies for Local Spin Density Calculations: A Critical Analysis. *Can. J. Phys.* **1980**, *58* (8), 1200–1211; (b) Lee, C.; Yang, W.; Parr, R. G. Development of the Colle-Salvetti Correlation-Energy Formula into a Functional of the Electron Density. *Phys. Rev. B* **1988**, *37* (2), 785–789.

(45) Frisch, M. J.; Trucks, G. W.; Schlegel, H. B.; Scuseria, G. E.; Robb, M. A.; Cheeseman, J. R.; Scalmani, G.; Barone, V.; Mennucci, B.; Petersson, G. A.; Nakatsuji, H.; Caricato, M.; Li, X.;

Hratchian, H. P.; Izmaylov, A. F.; Bloino, J.; Zheng, G.; Sonnenb, D. J. Gaussian, Inc., Wallingford, CT, **2009**.

(46) Dennington, Roy; Keith, Todd; Millam, J. GaussView, Version 5.0.9. Semichem Inc.,: KS 2009.